Food & Function

ROYAL SOCIETY OF CHEMISTRY

PAPER

View Article Online
View Journal

Cite this: DOI: 10.1039/d6fo00337k

Aged garlic extract suppressed macrophage-mediated inflammation in acute respiratory distress syndrome

Shun Nakazawa, [a] Shinsaku Togo,*[a] Chisato Tadokoro,[a] Soichiro Soma,[a] Yuta Arai,[a] Hiroaki Motomura,[a] Yuichi Nagata,[a] Takuto Sueyasu,[a] Haruki Hirakawa,[a] Koichi Kurata,[a,b] Issei Sumiyoshi,[a] Yusuke Ochi,[a] Junko Watanabe,[a] Hiroaki Ihara,[a] Kazuaki Hoshi,[a] Motoyasu Kato[a] and Kazuhisa Takahashi[a]

Background: Acute respiratory distress syndrome (ARDS) is a severe lung disorder characterized by intense pulmonary inflammation. Although corticosteroids are the primary anti-inflammatory therapeutic option, increased susceptibility to infection remains a significant clinical concern. Aged garlic extract (AGE) is a natural agent demonstrating anti-inflammatory and antioxidant qualities, and a high safety profile. We investigated the combined effect of AGE and low-dose steroids as a therapeutic approach through AGE-induced anti-inflammatory effects. *Methods*: Differentiated M1 macrophages were established by stimulating THP-1 cells with lipopolysaccharide (LPS) and interferon-gamma. We assessed inflammatory cytokine release and related signaling to investigate the effects of AGE and/or low-dose dexamethasone (DEX). We also assessed nuclear factor-kappa B (NF-κB) pathway activation using immunoblotting. We evaluated the therapeutic efficacy of AGE by monitoring body weight, quantifying inflammatory cells in the bronchoalveolar lavage fluid (BALF), and histological scoring of lung injury in an ARDS mouse model by intratracheal LPS instillation. *Results*: AGE significantly inhibited cytokines like Interleukin (IL)-6 and Monocyte chemoattractant protein-1 and suppressed NF-κB phosphorylation. Combining AGE with DEX broadened and enhanced inhibition of inflammatory mediators compared to monotherapy, while further suppressing NF-κB expression. In an ARDS model, the combination of AGE and DEX significantly suppressed LPS-induced body weight loss, inflammatory cell infiltration in BALF, and lung injury. *Conclusions*: Co-administration of AGE and low-dose DEX effectively suppressed excessive pulmonary inflammation in ARDS. This suggests a novel therapeutic approach that could enhance anti-inflammatory function, simultaneously reducing the adverse outcomes associated with high-dose steroid monotherapy.

Received 22nd January 2026,
Accepted 7th May 2026

DOI: 10.1039/d6fo00337k

rsc.li/food-function

Introduction

Acute respiratory distress syndrome (ARDS) is a serious clinical state exhibiting sudden and severe breathing failure, typically presenting with bilateral pulmonary infiltrates and arising from various pulmonary and extrapulmonary insults.[1,2] The reported mortality rate ranges from 18% to 54.7%.[3] A key feature of ARDS is excessive pulmonary inflammation driven by increased alveolar-capillary permeability, large-scale entry of polymorphonuclear neutrophils, as well as overabundant secretion of pro-inflammatory signaling molecules, ultimately leading to impaired gaseous exchange and respiratory insufficiency.[4] This excessive pulmonary inflammatory response is centrally mediated by immune cells known as macrophages. Typically, inactive M0 macrophages resident in the alveoli are responsible for pathogen surveillance and phagocytosis. Upon exposure to potent inflammatory signals such as Lipopolysaccharide (LPS) stimulation from ARDS, these M0 macrophages become activated *via* the NF-κB, p38/MAPK, and other pathways and differentiate into powerful pro-inflammatory M1 macrophages.[5–7] Large amounts of pro-inflammatory cytokines are generated and released by activated M1 macrophages, which initiate a cascade of further inflammatory reactions.[8] Among these, interleukin (IL)-6 and IL-1β are central to cytokine storm pathways, mediating fever and pulmonary inflammation by binding to Toll-like receptors.[9] Other key players include monocyte chemoattractant protein-1 (MCP-1) and IL-8, which further inflammation by recruiting monocytes and neutrophils, respectively.[10] Furthermore, tumor necrosis factor-α (TNF-α) contributes to the pathology by inducing cytotoxicity in epithelial and endo-

[a]*Department of Respiratory Medicine, Juntendo University Graduate School of Medicine, Tokyo, Japan. E-mail: shinsaku@juntendo.ac.jp; Tel: +81-3-3813-3111*
[b]*Drug Discovery Laboratory, Wakunaga Pharmaceutical Co., Ltd, Hiroshima, Japan*

thelial cells, thereby worsening edema.[11] Consequently, the activation of M1 macrophages and the subsequent release of cytokines are crucial mechanisms that exacerbate the severe pulmonary inflammation and tissue damage observed in ARDS.

To date, the administration of corticosteroids, such as dexamethasone (DEX), is the primary treatment for ARDS; they reduce the acute inflammatory responses.[12,13] However, clinical trials assessing the efficacy of corticosteroids in ARDS have yielded inconsistent results. Some demonstrate improved survival and ventilator-free days, while others have not found a clear mortality benefit, particularly when initiated late.[14,15] Moreover, the use of systemic corticosteroids is associated with significant side effects, such as the induction of a susceptible state owing to the diverse effects of corticosteroids,[16–18] a primary clinical concern in ARDS treatment. This highlights the persistent unmet need for safer therapeutic options with clear efficacy for ARDS. The severe inflammatory and oxidative stress components of ARDS have made antioxidant therapies attractive targets. However, numerous clinical trials of antioxidant agents, such as *N*-acetylcysteine and α-tocopherol, have failed to demonstrate significant improvements in patient outcomes or mortality, underscoring the challenge in translating anti-inflammatory and antioxidant strategies into effective ARDS treatments.[19,20]

In this research, we focused on the anti-inflammatory activities of aged garlic extract (AGE). AGE is derived from fresh garlic, resulting in an odorless preparation. It is characterized by the presence of water-soluble organosulfur compounds, including *S*-allylcysteine (SAC), *S*-allylmercaptocysteine (SAMC), and *S*-1-propenyl-cysteine, which have antioxidant properties.[21] The anti-inflammatory potential of AGE against neuroinflammation and renal injury,[22] neuroinflammation and cognitive dysfunction,[23] and hepatotoxicity has been demonstrated.[24] We hypothesize that AGE, unlike previously tested compounds, exerts its anti-inflammatory effects not merely by general scavenging but specifically by modulating key pathways, such as the NF-κB pathway, thereby suppressing the activation of M1 macrophages and inhibiting the subsequent transcription and release of major proinflammatory cytokines. Furthermore, we hypothesized that AGE would effectively prevent the tremendous inflammation caused by ARDS and might be effective with reduced DEX doses in combination therapy. Therefore, this research was designed to investigate the protective effects of AGE against LPS-induced ARDS and evaluate whether combining AGE with a low-dose steroid could enhance therapeutic efficacy while minimizing the risk of steroid-related complications.

Experimental methods

Preparation and characterization of AGE

AGE used in this study was prepared from organically grown garlic (*Allium sativum* L.) through a natural maturation process. Briefly, sliced raw garlic cloves were extracted using an aqueous ethanol solution and stored at room temperature for more than 10 months. This aging process facilitates the conversion of harsh and strong odor compounds into stable, water-soluble organosulfur compounds. To ensure the consistency of experimental results and eliminate batch-to-batch variation, a single lot of AGE was used throughout this research. The chemical characterization of the extract was performed by the manufacturer (Wakunaga Pharmaceutical Co., Ltd, Hiroshima, Japan). For sample preparation, a 2 mL aliquot of AGE was mixed with 2 mL of an internal standard (IS) solution (*S*-1-butenylcysteine, 0.5 mg mL^{-1} in 20 mM HCl) and 16 mL of 50% methanol. The mixture was shaken for 10 min and centrifuged at 2000 rpm for 10 min. The supernatant was diluted (1 : 10) with 50% methanol, filtered through a 0.22 μm membrane, and subjected to Liquid Chromatography-Mass Spectrometry (LC-MS) analysis using an UltiMate 3000 UHPLC system coupled with a Q-Exactive quadrupole-Orbitrap mass spectrometer (Thermo Fisher Scientific, Yokohama, Japan). A 1 μL aliquot was injected onto a Cadenza C18 column (150 mm × 2.1 mm, 3 μm; Imtact, Kyoto, Japan) at 40 °C. The mobile phase consisted of (A) 0.1% formic acid in water and (B) 0.1% formic acid in 80% methanol at a flow rate of 0.2 mL min^{-1}. The gradient elution was programmed as follows: 0–9 min, 0% B; 9–12 min, 0–40% B; 12–19 min, 40% B; 19–22 min, 40–100% B; 22–25 min, 100% B; 25–25.01 min, 100–0% B; and 25.01–32 min, 0% B. The bioactive constituents were identified and quantified using the following MS/MS transitions (*m*/*z*): 162.0577 > 73.0114 for SAC, 194.0304 > 73.0113 for SAMC, and 162.0577 > 145.0320 for *S*-1-propenyl-cysteine. The concentration of these compounds in the AGE lot was determined by comparing peak areas with those of authentic standardized samples (Table 1). Representative LC-MS chromatograms are provided in SI 1.

Dosage justification and human equivalent dose calculation

The dosages used in the *in vivo* and *in vitro* experiments were determined based on the pharmacokinetic profile of SAC, a primary bioactive marker of AGE. In humans, oral administration of 0.5 g of AGE (containing approximately 0.7 mg of SAC in the referenced study) has been reported to result in a peak plasma concentration (C_{max}) of approximately 18 ng mL^{-1} (0.11 μM),[25] with the area under the plasma concentration–time curve (AUC) of 0.43 mg h L^{-1}. In many clinical studies employing AGE, doses of 1 g or higher have been used; therefore, assuming linear pharmacokinetics, the C_{max} and AUC values of SAC are expected to be several-fold higher. In mice, oral administration of SAC at 50 mg kg^{-1} has been reported to yield a C_{max} of 12 μg mL^{-1} (75 μM),[26] with a corres-

Table 1 Chemical composition and concentrations of major allyl amino acids in the AGE

Compound	Concentration (mg per g-dry)
SAC	4.9
S-1-Propenyl-cysteine	4.8
SAMC	0.45

ponding AUC value of 18 mg h L^{-1}. In this *in vivo* study using an AGE dose of 2 g kg^{-1} (equivalent to 5 mg of SAC), the C_{max} and AUC of SAC are estimated to be approximately one-tenth of those observed at 50 mg kg^{-1}. Although the C_{max} in mice is substantially higher than that in humans, the total exposure levels of SAC are comparable between mice and humans because renal reabsorption of SAC is suggested to contribute more prominently in humans,[27] resulting in relatively higher systemic exposure. Therefore, the dose used in this study represents a slightly higher but physiologically relevant exposure to humans. *In vitro* assays, the concentrations were standardized to match the *in vivo* exposure: 2.5 mg mL^{-1} of AGE, 6.25 μg mL^{-1} (37.5 μM) of SAC, and 1.0 μg mL^{-1} (5.0 μM) of SAMC. These concentrations reflect the bioactive levels achieved following a potent therapeutic intake of AGE, allowing for the evaluation of its anti-inflammatory potential within a physiologically justifiable range.

Induction of M1 macrophages

Human monocytic leukemia THP-1 cells (ATCC, Manassas, VA, USA) were used because their morphological and differentiation properties are similar to those of primary monocytes and macrophages. To induce differentiation, THP-1 cells were seeded at a density of 5.0×10^5 cells per mL and then treated with 10 ng mL^{-1} of Phorbol 12-myristate 13-acetate (PMA; Selleck Chemicals, Houston, TX, USA, Cat. No. S7791) for 48 hours in RPMI 1640 supplemented with 10% Fetal calf serum (FCS; Sigma-Aldrich, St Louis, MO, USA) and Penicillin–streptomycin-amphotericin B (100 U mL^{-1}, 100 μg mL^{-1}, and 0.25 μg mL^{-1}, respectively, FUJIFILM Wako, Osaka, Japan, Cat. No. 161-23181). After PMA treatment, the culture supernatant was aspirated, and the cells were subsequently rinsed twice with prewarmed phosphate-buffered saline (PBS), followed by further incubation in PMA-free RPMI 1640 medium for an additional 48 h to obtain resting macrophages (M0 macrophages). To investigate the effects of AGE on macrophage differentiation, two experimental conditions were established: (i) M0 macrophages cultured without AGE (control group) and (ii) M0 macrophages cultured with AGE during the PMA-free incubation phase.

M1 macrophage differentiation was achieved using a previously described protocol.[28] In the control group, M0 macrophages were polarized into M1 macrophages by stimulation with 100 ng mL^{-1} LPS (O55:B5, Sigma-Aldrich, St Louis, MO, USA, Cat. No. L2880) and 20 ng mL^{-1} Interferon-γ (IFN-γ; PeproTech, Cranbury, NJ, USA, Cat. No. 300-02-20UG) with or without DEX (Wako Pure Chemical Industries, Tokyo, Japan, Cat. No. 040-30811) for 24 h. For the AGE-treated group, M0 macrophages pre-cultured with AGE were further stimulated with LPS and IFN-γ with or without DEX in the presence of AGE, maintaining their exposure throughout the polarization process.

Cell viability assay

To assess the potential cytotoxicity of AGE, an MTT assay was performed using THP-1-derived macrophages. THP-1 cells (1.0×10^4 cells per well) were seeded in 96-well plates and differentiated into M0 macrophages by treatment with 10 ng mL^{-1} PMA, followed by a 48 h recovery period. The cells were then incubated with various concentrations of AGE (1.0, 2.5, and 5.0 mg mL^{-1}) for 24 h. Cells treated with 10% Dimethyl sulfoxide (DMSO) served as a positive control for cytotoxicity. After incubation, 10 μL of MTT reagent (Sigma-Aldrich, St Louis, MO, USA, Cat. No. M2128) was added to each well and incubated at 37 °C for 4 h. The supernatant was then carefully aspirated, and the resulting formazan crystals were dissolved in 100 μL of DMSO. After shaking for 1 min using a plate mixer, the absorbance was measured at 570 nm using a microplate reader (iMark, Bio-Rad Laboratories, Hercules, CA, USA).

Flow cytometric analysis to detect M1 macrophages

Following experimental treatments (as described under "Induction of M0 and M1 macrophages"), THP-1-derived macrophages were detached using Accutase (Funakoshi, Tokyo, Japan, Cat. No. AT104) for 10 min at 37 °C. The cells were then washed twice with PBS and resuspended at a concentration of approximately 1.0×10^6 cells per mL in the same buffer. To exclude dead cells, cells were first stained with Zombie near-infrared (NIR) dye (BioLegend, San Diego, CA, USA, Cat. No. 77184) for 10 min in the dark at room temperature (20–25 °C) according to the manufacturer's protocol. After staining, cells were washed twice with PBS and pretreated with Fc Block (Immunostep, Salamanca, Spain, Cat. No. FCR-2ML) for 10 min at 4 °C to minimize non-specific antibody binding. Subsequently, cells were incubated for 30 min in the dark at 4 °C with the following fluorochrome-conjugated primary antibodies: anti-human CD11b-PE (BioLegend, Cat. No. 12-0118-42, Clone ICRF44) and anti-human CD80-Alexa Fluor® 647 (BioLegend, Cat. No. 305216, Clone 2D10). Finally, the cells were washed twice with PBS, resuspended in Fluorescence-Activated Cell Sorting (FACS) buffer (PBS containing 0.05% sodium azide and 0.5% BSA), and analyzed using an LSRFortessa flow cytometer (BD Biosciences, San Jose, CA, USA). Data were analyzed using FlowJo software (version 10.10.0; Tree Star, Ashland, OR, USA). The gating strategy was as follows: initial gates were set to exclude debris and doublets based on forward scatter area *versus* forward scatter height plots. Live cells were then identified by gating on the Zombie NIR dye-negative population. Within the live single-cell population, macrophages were identified by gating on CD11b-positive cells. Finally, the percentage of CD80-positive cells and the mean fluorescence intensity (MFI) of CD80 were determined within the CD11b-positive cells.

Real-time PCR quantification for cytokine production

Reverse transcription of the purified RNA to cDNA was performed with the aid of a High-Capacity cDNA Reverse Transcription Kit, which included RNase Inhibitors (Thermo Fisher Scientific, Waltham, MA, USA; Cat. No. 4374966), with 500–1000 ng of starting RNA per reaction. Quantitative polymerase chain reaction (qPCR) was carried out using the StepOnePlus™ Real-Time PCR System with SYBR Green qPCR Master Mix (Thermo Scientific, Waltham, MA, USA; Cat. No.

A66732). The qPCR data were analyzed using the $2^{-\Delta\Delta Ct}$ method, with M0 macrophage RNA serving as the control. The primers used to measure the cytokine production level are listed below (Table 2).

Enzyme-linked immunosorbent assay for inflammatory cytokines measurement

After the designated experimental treatment period, the cell culture supernatants were collected from each well. Centrifugation proceeded at 12 000 rpm for 10 min at 4 °C; this step served to pellet cellular debris. The supernatants were immediately stored at −80 °C until further analysis. Various inflammatory cytokine levels present in the cell culture media were quantified using the commercial enzyme-linked immunosorbent assay (ELISA) kits listed below.

Multiplex cytokine analysis. Initially, a multiplex ELISA platform was used to simultaneously quantify multiple inflammatory cytokines. IL-6, IL-1β, and TNF-α levels were measured using a custom ProcartaPlex Human Cytokine/Chemokine Panel (Thermo Fisher Scientific, Waltham, MA, USA; Product No. PPX-06430949-000). Briefly, the cell culture supernatants were diluted (1 : 2) with the assay diluent and added to the wells. Subsequently, 50 μL of the diluted samples or standards were added to the wells containing magnetic beads conjugated with capture antibodies and incubated for 2 h at room temperature. After washing, detection antibodies were applied and incubated for 1 h. Streptavidin-phycoerythrin was added, after another wash, and the cells were incubated for 30 min. The beads were analyzed using a Luminex 200 system (Luminex Corporation, USA).

Single-Plex ELISA for IL-8 and MCP-1. As IL-8 and MCP-1 levels fell outside the detection range or standard curve in the multiplex analysis, their concentrations were subsequently determined using an ELISA kit, according to the manufacturer's protocol: IL-8 (Thermo Fisher Scientific, Waltham, MA, USA, Cat. No. 88-8086-86); MCP-1: (Thermo Fisher Scientific, Waltham, MA, USA, Cat. No. 88-7399-88). Briefly, 96-well microplates pre-coated with capture antibodies were incubated with 100 μL of standards or diluted samples (IL-8 samples were diluted 1 : 150, and MCP-1 samples were diluted 1 : 400) for 2 h at room temperature. After washing the wells three times with Wash Buffer, 100 μL of Horseradish peroxidase-conjugated detection antibody was applied to each well and incubated for 1 h at room temperature. After an additional sequence of washing steps, 100 μL of TMB substrate was applied to each well and incubated in the dark for 15 min. The reaction was then stopped by applying 50 μL of stop solution (1 M sulfuric acid), and the absorbance was measured immediately at 450 nm using a SpectraMax ABS Plus microplate reader (Molecular Devices, San Jose, CA, USA). The concentrations of the cytokines were calculated using a standard curve from serially diluted recombinant cytokine standards provided with the kit.

Western blot analysis to detect AGE-mediated anti-inflammatory signals

Western blot assays were performed to evaluate protein expression in macrophages. First, cells were lysed with a radioimmunoprecipitation assay Buffer (FUJIFILM Wako Pure Chemical Corporation, Osaka, Japan; Cat. No. 182-02451) supplemented with an HAlt phosphatase inhibitor cocktail (Thermo Fisher Scientific, Waltham, MA, USA; Cat. No. 78428) and a protease inhibitor cocktail (Roche, Basel, Switzerland, Cat. No. 11836153001). After centrifugation at 12 000 rpm for 10 min at 4 °C, the supernatant was collected. Protein levels were measured using the Bicinchoninic acid assay Protein Assay Kit (Thermo Fisher Scientific, Waltham, MA, USA, Cat. No. 23225). Equal amounts of protein (10 μg) were separated by SDS-PAGE using the 7.5% and 12% TGX FastCast Acrylamide Kit (Bio-Rad Laboratories, Hercules, CA, USA, Cat. No. 1610171 and 1610175). The separated proteins were electrotransferred onto *trans*-Blot Turbo Mini-Size PVDF membranes (Bio-Rad Laboratories, Hercules, CA, USA, Cat. No. 1704272). The membranes were blocked with a PVDF Blocking Reagent (TOYOBO, Osaka, Japan, Code No. NYPBR01) or Skim milk (BD Difco™ Skim Milk; Becton, Dickinson and Company, Cat. No. 232100) for 1 h at room temperature. The membranes were incubated overnight at 4 °C with primary antibodies. Primary antibodies against the following proteins were used for immunoblotting: Anti-NF-kB p65 antibody [E379] (1 : 1000; Abcam, Cambridge, UK, Cat. No. ab32536), anti-Phospho-NF-κB p65 [Ser536] [93H1] (1 : 1000; Cell Signaling Technology,

Table 2 Primer sequences used for qPCR analysis

Target	Sense primer (5′-3′)	Antisense primer (5′-3′)
IL-6	AGACAGCCACTCACCTCTTCAG	TTCTGCCAGTGCCTCTTTGCTG
IL-8	ACTGAGAGTGATTGAGAGTGGAC	AACCCTCTGCACCCAGTTTTC
CD80	CTCTTGGTGCTGGCTGGTCTTT	GCCAGTAGATGCGAGTTTGTGC
IL-1β	CCACAGACCTTCCAGGAGAATG	GTGCAGTTCAGTGATCGTACAGG
TNF-α	CTCTTCTGCCTGCTGCACTTTG	ATGGGCTACAGGCTTGTCACTC
MCP-1	CATGAAAGTCTCTGCCGCCC	GGGCATTGATTGCATCTGGCTG
GAPDH	GTCTCCTCTGACTTCAACAGCG	ACCACCCTGTTGCTGTAGCCAA
CD163	CCAGAAGGAACTTGTAGCCACAG	CAGGCACCAAGCGTTTTGAGCT
CD206	AGCCAACACCAGCTCCTCAAGA	CAAAACGCTCGCGCATTGTCCA
IL-10	TCTCCGAGATGCCTTCAGCAGA	TCAGACAAGCCTTGGCAACCCA
TGF-β	TACCTGAACCGGTGTTGCTCTC	GTTGCTGAGGTATCGCCAGGAA

USA, Cat. No. 3033), anti-inhibitor of nuclear factor kappa-B alpha(IκBα) (1 : 1000; Cell Signaling Technology, USA, Cat. No. 9242), GAPDH (1 : 1000; FUJIFILM Wako, Osaka, Japan, Cat. No. 016-25523). The following day, the membranes were incubated with anti-mouse IgG (1 : 10000, Sigma-Aldrich, St Louis, MO, USA, Cat. No. NA931) or anti-rabbit IgG (1 : 10000, Sigma-Aldrich, St Louis, MO, USA, Cat. No. 934), for 1 h. Visualization of the bound antibodies was achieved with peroxidase-conjugated secondary antibodies and enhanced chemiluminescence using a ChemiDocTM Imaging System (Bio-Rad Laboratories Inc., Hercules, CA, USA, Cat. No. 170-5061). Band intensity was analyzed using the Image Lab software 6.0.1 (Bio-Rad Laboratories Inc.).

ARDS model animals and experimental design

Male C57BL/6J mice (8–10 weeks old, ~25 g) were purchased from Oriental Yeast Co., Ltd (Tokyo, Japan). Mice were maintained in a specific pathogen-free environment under controlled conditions (25 °C, 12 h light/dark cycle) with free access to food and water. All animal experiments were approved by the Animal Care and Use Committee of Juntendo University (Approval No. 2024300) and performed in accordance with the institutional and National Institutes of Health guidelines.

Mice were randomly assigned to four experimental groups stratified by body weight. All the mice received a single intratracheal instillation of LPS (20 mg kg^{-1}). This procedure established the ARDS model, consistent with previously reported methods.[29,30] Twelve mice from each group were used to assess changes in body weight. Group A (control) received an intraperitoneal (i.p.) injection of PBS and oral distilled water (DDW; 10 mL kg^{-1}). Group B received an i.p. injection of DEX (1 mg kg^{-1}) and oral DDW. Group C received i.p. PBS and oral AGE (2 g kg^{-1}), whereas Group D received an i.p. injection of DEX (1 mg kg^{-1}) and oral AGE. AGE or DDW was administered orally once daily for 2 days prior to LPS instillation and continued thereafter. DEX (Wako Pure Chemical Industries, Tokyo, Japan, Cat. No. 040-30811) was administered i.p. once daily starting on the day of LPS instillation. The administration volume for both oral and i.p. treatments was consistently 10 mL kg^{-1} across all groups to ensure equal solvent exposure. Body weight was monitored daily, and the percentage change in body weight was calculated until day 4. Any mice that died prematurely or were excluded due to technical failure were excluded from the analysis. The final number of animals analyzed in each group is visually represented by individual data points within the figures.

Bronchoalveolar lavage fluid (BALF) and histological evaluations were performed on five-six mice from each group following the same treatment protocol. BALF samples were collected according to a previously described method.[31] The mice were euthanized by inhalation of 5% isoflurane. BALF was collected by cannulating the trachea and lavaging the lungs twice with sterile saline (1.0 mL, twice). Total cell counts were determined using Türk's solution, and differential cell counts were performed on cytospin preparations stained with Diff-Quik (Sysmex International Reagents, Kobe, Japan, Cat. No. 16920). Lung tissues were fixed in 10% neutral-buffered formalin, embedded in paraffin, and sectioned at 3 μm. These tissue slices were then stained using Hematoxylin and Eosin (HE). Both the differential cell counts of BALF and the histological evaluations of lung tissues were blinded by two independent observers (SN and SS). For the lung tissues, histological scoring was conducted based on previously established criteria.[32]

Statistical analysis

Data are expressed as the mean ± standard deviation. A one-way analysis of variance followed by Tukey's multiple comparisons test was used for comparisons involving three or more groups. GraphPad Prism 9 (GraphPad Inc., San Diego, CA, USA) was used to create the column graphs and perform statistical analyses. Statistical significance was set at $p < 0.05$.

Results

AGE and DEX reduce the expression of MCP-1 in M1 macrophages

Given the critical role of MCP-1 in monocyte recruitment and M1 macrophage polarization during inflammation, we assessed MCP-1 mRNA expression by RT-PCR in cells treated with various concentrations of DEX (1 μg mL^{-1}, 100 ng mL^{-1}, 10 ng mL^{-1}, and 1 ng mL^{-1}).[33] Our results demonstrated a clear dose-dependent inhibition of MCP-1 mRNA expression by DEX. While DEX at 1 ng mL^{-1} exhibited a modest suppression of inflammatory responses, higher concentrations (100 ng mL^{-1} and 1 μg mL^{-1}) induced potent anti-inflammatory effects, with the fold change of MCP-1 mRNA expression reaching a near-saturated level. Based on these findings, and with the aim of investigating a potential steroid-sparing effect through combination therapy, 1 ng mL^{-1} DEX was identified as a suboptimal or partially effective concentration for anti-inflammatory action in our *in vitro* model (SI 2a).

Next, we evaluated the anti-inflammatory dose–response of AGE by treating cells with various concentrations (0.5, 1.5, and 2.5 mg mL^{-1}) and measuring MCP-1 mRNA expression. Treatment with AGE at 2.5 mg mL^{-1} resulted in a significant reduction in the fold-change of MCP-1 mRNA compared to the control group ($p = 0.0275$; SI 2b). Following the identification of 2.5 mg mL^{-1} as the effective concentration, we performed an MTT assay to confirm that this dose did not induce non-specific cytotoxicity. The results showed that AGE at concentrations up to 5.0 mg mL^{-1} maintained cell viability comparable to the untreated control, whereas 10% DMSO significantly reduced viability (SI 2c). These findings ensure that the observed anti-inflammatory effects of AGE at 2.5 mg mL^{-1} were not due to impaired cell viability, demonstrating a favorable safety profile within the dose range used in this study. Consequently, this concentration of AGE was used in the subsequent experiments with DEX.

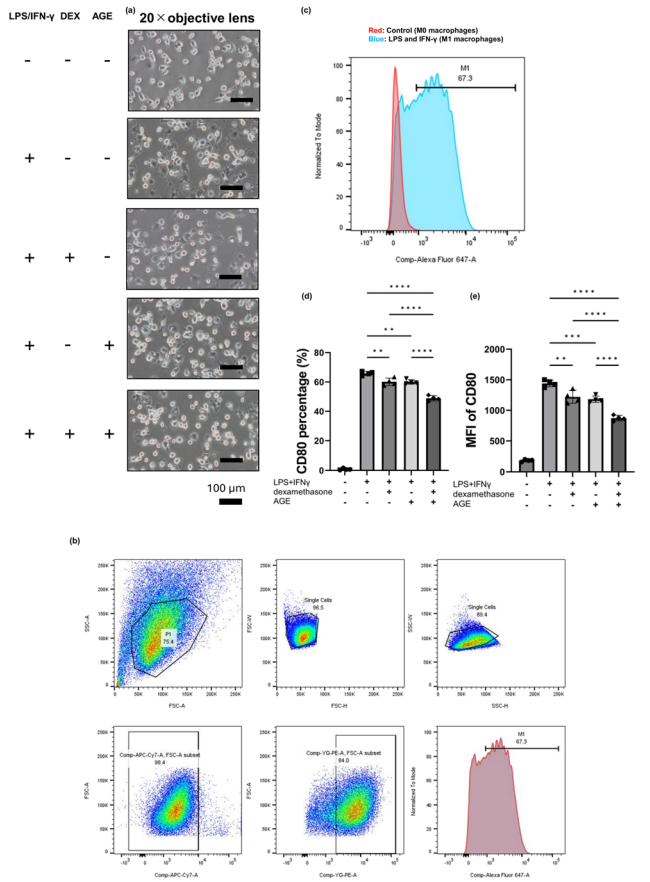

Fig. 1 Morphological changes and CD80 expression. Representative bright-field microscopy images of THP-1 macrophages after PMA differentiation and subsequent treatment. (a) Morphology of M0 macrophages, morphology of M1 macrophages, M1 macrophages treated with DEX, M1 macrophages treated with AGE, and M1 macrophages treated with DEX and AGE. All images were taken at ×20 objective lens. Scale bar, 100 μm. All images are representative of at least three independent experiments. The expression of CD80 in THP-1-derived macrophages was analyzed using flow cytometry. (b) Representative flow cytometry plots illustrating the gating strategy used for the M1 macrophages. After excluding doublets and dead cells (identified by NIR Zombie dye), live cells were gated on the CD11b-positive population. Within the CD11b-positive population gate, the percentage of CD80-positive cells was determined. (c) Representative histograms showing the overlay of CD80 expression on M0 and M1 macrophages, demonstrating the induction of CD80 expression upon M1 polarization. (d) The percentage of CD80-positive cells and (e) the mean fluorescence intensity (MFI) of CD80 in the CD11b-positive population were quantified. Data were calculated as the mean ± standard error of the mean (SEM) and analyzed using one-way ANOVA. *$p < 0.05$, **$p < 0.01$, ***$p < 0.001$, and ****$p < 0.0001$. PMA, Phorbol 12-myristate 13-acetate; DEX, dexamethasone; NIR, near-infrared; MFI, mean fluorescence intensity; SEM, standard error of the mean; AGE, aged garlic extract; ANOVA, analysis of variance.

Morphological change of macrophage cells after DEX and AGE treatment

Morphological changes in THP-1 macrophages after various treatments were examined using bright-field microscopy. As shown in Fig. 1a, unstimulated M0 macrophages exhibited a relatively circular morphology with smooth boundaries, and pseudopod formation was rarely observed. In contrast, LPS and IFN-γ induced M1 macrophages showed a clear morphological change, displaying numerous elongated pseudopods and an irregular cell shape. Following co-treatment with DEX or AGE, the macrophages still showed pseudopod formation, suggesting that these treatments alone did not fully suppress the morphological changes associated with M1 macrophage activation. However, combined treatment with DEX and AGE resulted in a strong suppression of these morphological changes, with fewer cells exhibiting pseudopods compared to the single-treated groups.

AGE enhances the effects of DEX on the reduction of cellular CD80 expression in M1 macrophages

Flow cytometry was used to evaluate the expression of the M1 macrophage-specific marker CD80 in THP-1-derived macrophages (Fig. 1b and c). Treatment with AGE alone significantly reduced the percentage of CD80 positive cells (p = 0.0045 *vs.* positive control; Fig. 1d) and CD80 MFI (p = 0.0005 *vs.* positive control; Fig. 1e). Furthermore, co-administration of DEX with AGE resulted in an even greater reduction in both the percentage of CD80 positive cells ($p < 0.0001$; Fig. 1d) and CD80 MFI ($p < 0.0001$; Fig. 1e) compared to AGE treatment alone.

AGE synergistically enhances the effect of DEX on the suppression of inflammatory cytokine release

FACS analysis showed that AGE suppressed the expression of the M1-macrphage-specific cellular surface marker CD80, suggesting the restoration of the M0-macrphage phenotype (Fig. 1d and e). Subsequently, the effects of AGE on the expression of inflammatory cytokines, with or without co-incubation with DEX, were analyzed in terms of mRNA expression. RT-PCR revealed significant alterations in the mRNA expression levels of several proinflammatory markers. As shown in Fig. 2a–e, treatment with AGE alone significantly suppressed the mRNA levels of IL-6, IL-1β, and MCP-1 ($p <$ 0.0001, 0.0005, and 0.0077, respectively), while a similar downward trend was observed for IL-8 and TNF-α (p = 0.4339 and p = 0.0691). Furthermore, co-administration of DEX and AGE resulted in a more pronounced reduction in these mRNA levels compared to the positive control (LPS + IFN-γ) ($p <$ 0.0001 for IL-6 and MCP-1, p = 0.0002 for IL-8; p = 0.0001 for IL-1β; p = 0.0078 for TNF-α). This combined effect highlighted the potential of AGE to enhance the anti-inflammatory efficacy of suboptimal doses of DEX. Compared to AGE treatment alone, the combination therapy further suppressed mRNA expression, with significant differences observed for IL-8 (p = 0.00023) and MCP-1 (p = 0.0156), while IL-6, IL-1β, and TNF-α showed similar downward trends (p = 0.4158, 0.7283, and 0.6288, respectively). In addition to cytokine analysis, AGE treatment alone significantly reduced CD80 mRNA expression (Fig. 2f). The co-administration of DEX and AGE led to a greater reduction compared to the positive control (p = 0.0003), although the further reduction compared to AGE

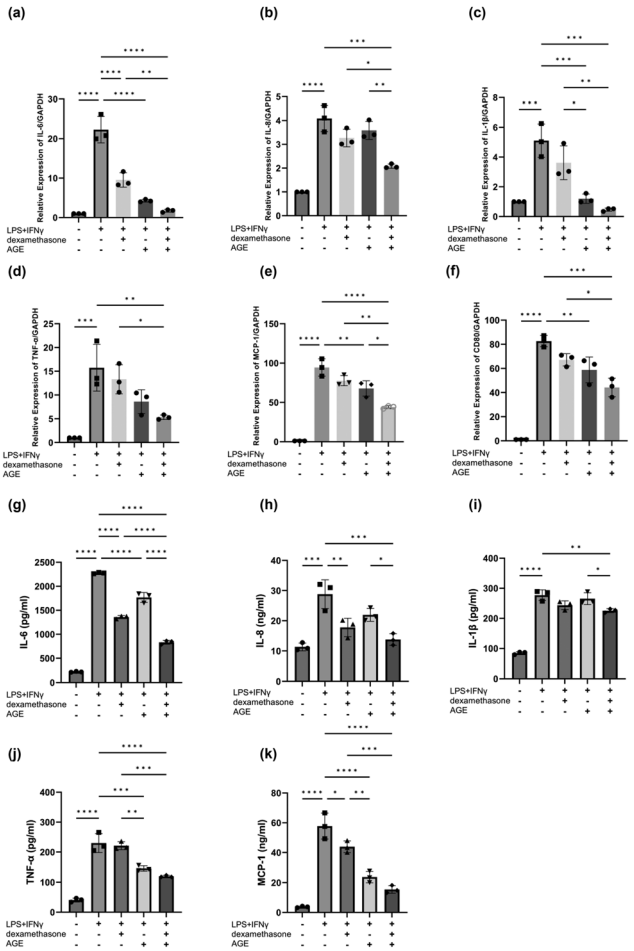

Fig. 2 Effects of AGE and DEX on inflammatory marker expression in macrophages. The mRNA expression levels of (a) IL-6, (b) IL-8, (c) IL-1β, (d) TNF-α, (e) MCP-1, and (f) CD80 were quantified by quantitative RT-qPCR. Expression levels were normalized to the GAPDH mRNA levels. The protein levels of (g) IL-6, (h) IL-8, (i) IL-1β, (j) TNF-α, and (k) MCP-1 were measured in cell culture supernatants by ELISA. Data were calculated as the mean ± SEM and analyzed using a one-way ANOVA. *p < 0.05, **p < 0.01, ***p < 0.001, and ****p < 0.0001. SEM, standard error of the mean; ANOVA, analysis of variance; ELISA, enzyme-linked immunosorbent assay; TNF-α, tumor-necrosis factor alpha; GAPDH, glyceraldehyde 3-phosphate dehydrogenase; RT-PCR, real-time polymerase chain reaction.

alone did not reach statistical significance (p = 0.1270). To corroborate these findings at the protein level, we performed ELISA for key inflammatory cytokines in the cell culture supernatants. LPS and IFN-γ stimulation significantly increased the production of all analyzed cytokines. While AGE or DEX alone showed significant or partial suppression, the combined treatment (DEX + AGE) led to a markedly greater suppression compared to the positive control (p < 0.0001 for IL-6, TNF-α, and MCP-1; p = 0.0006 for IL-8; p = 0.0074 for IL-1β). Notably, compared to AGE treatment alone, the combination therapy further significantly reduced the protein levels of IL-6 (p < 0.0001), IL-8 (p = 0.0389), and IL-1β (p = 0.0349), whereas TNF-α and MCP-1 levels remained comparable between the two groups (p = 0.3274 and 0.2735, respectively) (Fig. 2g–k). Furthermore, to investigate whether AGE also promotes a shift toward an anti-inflammatory phenotype, we analyzed the mRNA expression of M2 macrophage markers, including CD163, CD206, Transforming Growth Factor-beta (TGF-β), and IL-10 (SI 3). The co-administration of DEX and AGE significantly up-regulated the mRNA expression of CD163 and CD206 compared to the positive control (LPS and IFN-γ-stimulated group) (p = 0.0002, and <0.0001, respectively). Notably, this combination therapy also showed a significant increase in these markers compared to AGE treatment alone (p = 0.0047 for CD163; p < 0.0001 for CD206), demonstrating a synergistic effect in promoting M2 polarization. Regarding TGF-β and IL-10, the combined treatment resulted in a significant up-regulation compared to the positive control (p = 0.025 for TGF-β; p = 0.0124 for IL-10). Although the combination of DEX and AGE did not significantly increase TGF-β and IL-10 levels compared to AGE alone (p = 0.5142 and p = 0.0810, respectively), the DEX + AGE group exhibited a modest upward trend in the expression of both cytokines.

Combination of AGE and DEX suppressed NF-κB signaling

First, a time-course study was conducted to evaluate the peak expression of phosphorylated (p)-NF-κB. The p-NF-κB/total (t)-NF-κB ratio peaked at 45 min, which was used as the time point for subsequent experiments (Fig. 3a). The main analysis revealed that all treatment groups exhibited a significant decrease in the p-NF-κB/t-NF-κB ratio compared to the control group (M1 macrophages) (Fig. 3b and c). Notably, combined AGE and DEX treatment resulted in a more pronounced suppression of NF-κB phosphorylation than the control group (p = 0.0007). While the combination therapy showed a trend toward greater suppression than treatment with AGE or DEX alone, the difference between AGE alone and the DEX + AGE group did not reach statistical significance (p = 0.7150). Similarly, a time-course study of IκBα showed that it degraded most rapidly at 30 min (Fig. 3d). Consistent with the NF-κB results, both AGE and DEX treatments led to greater preservation of IκBα compared to the control group (Fig. 3e and f). The co-administration of DEX and AGE significantly inhibited IκBα degradation compared to the control group (p = 0.0293), although no significant difference was observed when compared to AGE treatment alone (p = 0.6284). These results suggest that combined therapy effectively inhibits NF-κB signaling by preventing IκBα degradation. The uncropped blots for these experiments are shown in SI 4.

AGE and DEX attenuated LPS-induced lung injury in the ARDS model mice

Despite the administration of a high dose of LPS, the mortality rate was very low (<10%) across all groups, indicating that a lethal model was not achieved in the present study. Consequently, the body weight change was used as the primary endpoint to assess disease severity. Based on previous studies, day 4 was selected as the time point for evaluation of acute inflammation.[34] This day represents the peak of acute

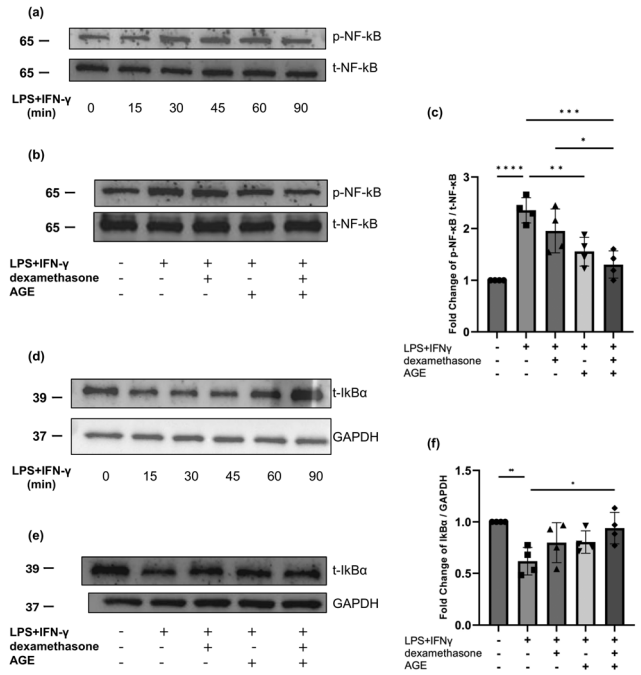

Fig. 3 Effect of LPS and IFN-γ on NF-κB and IkBα signaling in macrophages. (a) Immunoblot analysis of time-dependent NF-κB phosphorylation in M0 macrophages. Cells were stimulated with LPS and IFN-γ for the indicated periods (0–90 min), and the phosphorylation status of NF-κB NF-κB was determined. (b) Representative immunoblot of phosphorylated (p)-NF-κB/total (t)-NF-κB from M0 macrophages stimulated with LPS and IFN-γ for 45 min. (c) Quantification of the immunoblot shown in (b). The fold change of p-NF-κB/t-NF-κB was calculated relative to the unstimulated control. (d) Immunoblot analysis of time-dependent IkBα in M0 macrophages. Cells were stimulated with LPS and IFN-γ for the indicated periods (0–90 min), and the status of IkBα was determined. (e) Immunoblot analysis of IkBα/GAPDH in M0 macrophages stimulated for 30 min. (f) Quantification of the immunoblot shown in (e). The relative protein level of IkBα was normalized to GAPDH. Data were calculated as the mean ± SEM and analyzed using one-way ANOVA. *p < 0.05, **p < 0.01, ***p < 0.001, and ****p < 0.0001. LPS, lipopolysaccharide; ANOVA, analysis of variance; SEM, standard error of mean; GAPDH, glyceraldehyde 3-phosphate dehydrogenase.

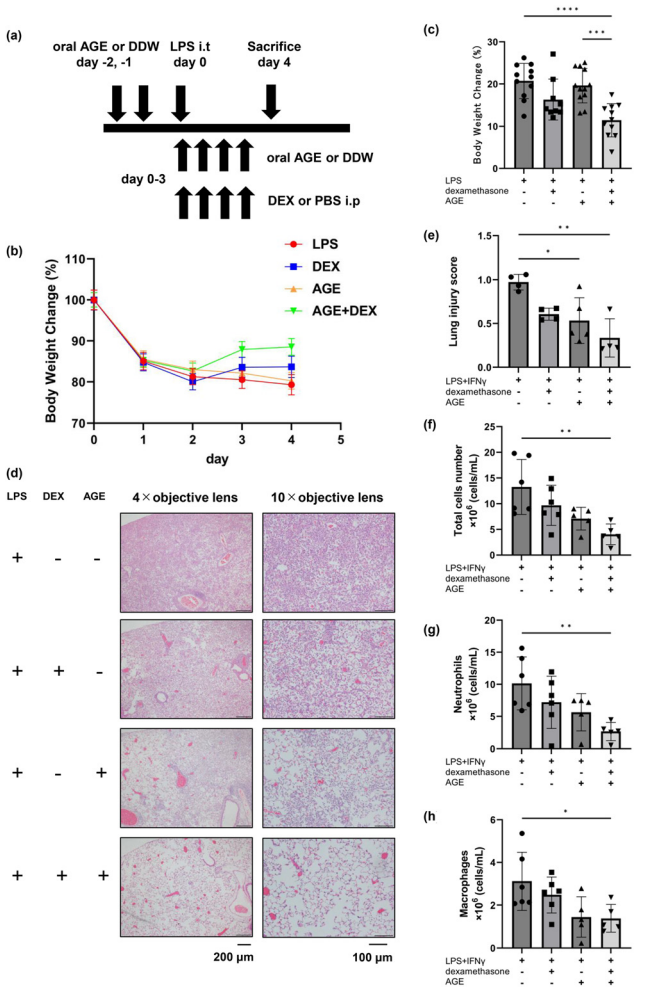

Fig. 4 Effect of AGE and DEX on a mouse model of LPS-induced lung injury. (a) A schematic representation of the experimental design. Mice were given an oral gavage of either AGE or DDW for two days prior to the intratracheal instillation of LPS on day 0. Thereafter, oral administration of AGE or DDW, along with an i.p. injection of either DEX or PBS, continued until day 3, when the mice were euthanized for subsequent analysis. (b) The percentage change in body weight was monitored daily for all experimental groups. Body weight was normalized to 100% on Day 0 (the day of LPS instillation). (c) A bar graph showing the mean percentage body weight change for each group on day 4 (n = 12 in each group). (d) HE-stained lung specimens on day 4. Bars, 200 μm and 100 μm. Representative images of whole lung sections are shown in SI 3A–D. (e) Lung injury scores on days 4 (n = 5 in each group). (f–h) Concentrations of inflammatory cells (total cells, neutrophils, and macrophages) in the BALF of each group on day 4 (n = 6 in each group). Data were calculated as the mean ± SEM and analyzed using one-way ANOVA. *p < 0.05, **p < 0.01, ***p < 0.001, and ****p < 0.0001. LPS, lipopolysaccharide; DEX, dexamethasone; AGE, aged garlic extract; RT-PCR, real-time polymerase chain reaction; ANOVA, analysis of variance; SEM, standard error of mean; GAPDH, glyceraldehyde 3-phosphate dehydrogenase; IFN-γ, interferon gamma.

lung injury, characterized by maximal body weight loss and cellular infiltration. Body weight loss, BALF analysis, and histopathological assessment of the lung tissue were performed. To examine the anti-inflammatory properties of AGE and DEX, a murine lung injury model was established by intratracheal LPS instillation (Fig. 4a). Prior to the main study, preliminary experiments were conducted to determine an appropriate dose of DEX to serve as a positive control demonstrating a minimal therapeutic effect, allowing for the clear assessment of the added benefit of AGE. We compared the effect of various DEX doses (1, 2, and 3 mg kg^{-1}) on the time course of body weight change following LPS-induced ARDS. As shown in SI 5, the 1 mg kg^{-1} dose was selected because it resulted in a less pronounced improvement in body weight loss over 4 days compared to the higher doses, thereby providing a suitable baseline effect for comparison with combination treatments. The administration of AGE and DEX significantly restored LPS-induced body weight loss on day 4 compared to the positive control (p < 0.0001; Fig. 4b and c). Notably, combination therapy resulted in a significantly greater improvement in body weight than AGE treatment alone (p = 0.0002). Consistent

with these results, mice treated with the combination of AGE and DEX exhibited improved cellular infiltration and a significantly reduced lung injury score compared to the positive control (p = 0.0017; Fig. 4d and e; SI 6). Additionally, the combined AGE and DEX treatment effectively reduced the numbers of total cells, neutrophils, and macrophages in the BALF compared to the positive control (p = 0.0038, 0.0095, and 0.0453, respectively; Fig. 4f–h). Although the further reduction in these cellular parameters by the combination therapy compared to AGE treatment alone did not reach statistical significance (p = 0.5840, 0.5223, and 0.9996, respectively), the DEX + AGE group exhibited a consistent downward trend in the infiltration of total cells, neutrophils, and macrophages.

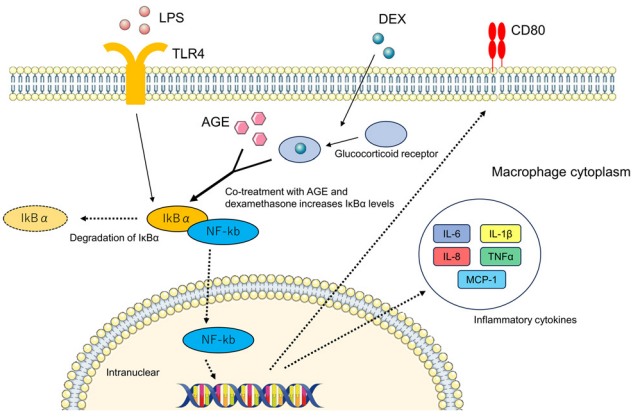

Fig. 5 AGE and DEX suppressed lung inflammation *via* NF-κB signaling. The combination of dexamethasone and AGE exhibited a potent anti-inflammatory effect during the acute inflammatory phase by suppressing the NF-κB pathway, leading to the inhibition of pro-inflammatory cytokine production and CD80 expression. Schematic representation of the signaling pathway. This figure was created by modifying the elements of Servier Medical Art (smart.servier.com). AGE, aged garlic extract.

Discussion

We demonstrated for the first time that the co-administration of AGE and low-dose DEX synergistically suppresses inflammation that cannot be adequately controlled by steroid monotherapy. This combination resulted in attenuated weight loss, a reduction in the number of inflammatory cells in the BALF, and an improvement in the histological lung injury score in ARDS model mice. The expression of key pro-inflammatory cytokines released from M1-macrophages was strongly inhibited by combined treatment. Additionally, we confirmed several key mechanistic insights, including the suppression of CD80 expression, a surface marker for M1 macrophages known to be a crucial co-stimulatory signaling molecule,[35–37] and the inactivation of the NF-κB pathway. Taken together, these results suggest that the combination of AGE and DEX effectively mitigates the excessive inflammatory response characteristic of ARDS *via* multiple complementary mechanisms.

Previous studies have reported the anti-inflammatory properties of AGE from various perspectives;[38,39] for instance, one study demonstrated its inhibitory effect on the production of inflammatory cytokines, such as IL-6 and IL-8, induced by SARS-CoV-2 infection.[40] The anti-inflammatory effect observed in this study is consistent with numerous prior reports that demonstrate AGE's ability to suppress the NF-κB pathway.[41–43] It has been reported that SAC, a constituent of AGE, inhibits NF-κB activation through multiple mechanisms, including an effect on IκBα *via* MAP kinases and a potent inhibitory effect on Inhibitor of nuclear factor kappa-B kinase subunit beta kinase, which prevents IκBα phosphorylation.[41,44] In addition to these mechanisms, our results suggest that AGE containing SAC may increase the expression of IκBα through various signals (Fig. 5), and the combination of these effects may lead to the suppression of the NF-κB pathway. Furthermore, AGE treatment significantly up-regulated the mRNA expression of M2 marker IL-10. While the increases in other markers, such as CD163 and TGF-β associated with the pro-resolving M2a and M2c phenotypes, respectively[45] did not reach statistical significance, they followed a consistent upward trend. These results are consistent with a previous report by Miki *et al.*, which demonstrated that *S*-1-propenyl-cysteine, a key constituent of AGE, promotes M2c-like polarization.[46] Notably, the combination of AGE and DEX exerted a much more potent effect, significantly up-regulating all examined M2 markers and anti-inflammatory cytokines. These findings indicate that the combined treatment likely exerts its therapeutic effects through a dual mechanism: the potent inhibition of M1 activation and the promotion of a reparative M2-like phenotype.

Recently, the use of naturally derived substances such as natural herbs as an alternative to steroids has gained attention in basic research because of their unique advantages, including fewer side effects, diverse mechanisms of action, and abundant availability,[47] although their acceptance in clinical practice is currently limited due to the lack of high-quality human clinical research. Therapeutic strategies that combine other drugs, such as immunosuppressants in the treatment of interstitial pneumonia, to reduce steroid dosage due to side effects are widely applied in clinical practice.[48,49] Considering this, the combination of steroids and naturally derived substances can be considered a rational treatment strategy. Our finding of its synergistic effect with low-dose DEX in ARDS suggests that the anti-inflammatory properties of AGE demonstrated in these preliminary studies are effective even in the critical state of ARDS. This method has the potential to contribute to the refinement of existing standard treatments. Thus, this study broadens the scope of therapeutic applications of AGEs in the context of respiratory diseases.

This study has some limitations. First, we did not evaluate long-term or major clinical outcomes of ARDS. While the LPS-induced model is a validated screening tool, it does not fully recapitulate the complex and heterogeneous nature of human ARDS. Specifically, it often fails to capture key clinical features such as extensive epithelial injury, coagulation abnormalities, and fibroproliferation.[50–52] Furthermore, as our experimental protocol did not achieve a lethal model, it should be character-

ized as a mild-to-moderate injury model. Therefore, caution is required when extrapolating the therapeutic efficacy of AGE and DEX observed here to severe or lethal clinical ARDS. In addition to the limitations of the *in vivo* model, the physiological relevance of the AGE concentration used in our *in vitro* experiments must be addressed. Although our MTT assay confirmed that this concentration did not affect cell viability up to 5.0 mg mL^{-1}, it is relatively high compared to typical human plasma levels. There is an inherent gap between static *in vitro* environments and the dynamic absorption, distribution, metabolism, and excretion processes in a living organism. While peak concentrations of AGE constituents in mice can be substantially higher than those in humans, the direct translatability of these high *in vitro* doses to clinical settings remains a challenge. Finally, as the AGE used in this study contains a variety of compounds that may affect multiple signaling pathways, further investigation is needed to identify the specific active components and their precise underlying mechanisms in more advanced models before proceeding to clinical trials.

Conclusions

This study demonstrates that adding AGE to low-dose steroids could maximize the anti-inflammatory effects in ARDS, proposing a novel strategy for improving steroid therapy by avoiding its adverse effects. While the optimal role of steroid therapy in ARDS remains debatable, these results suggest a new potential complementary treatment option. However, further verification is required to facilitate its clinical application.

Author contributions

SN: conceptualization, methodology, formal analysis, investigation, writing – original draft preparation, and funding acquisition for the study. ST: conceptualization, methodology, and was a major contributor to investigation. MK: conceptualization, methodology, and was a major contributor to investigation. CT, SS, YA, and HM: contributed to data curation. KK contributed to data curation and was also a major contributor to investigation. HI: performed formal analysis. KH: major contributor to formal analysis. YN: performed the investigation. KT: was a major contributor to investigation. TS and HH were major contributors to the writing – original draft preparation. YO, IS, and JW: were major contributors to funding acquisition. All authors read and approved the final manuscript.

Ethics approval and consent to participate

ARRIVE guidelines were strictly followed for this study. Animal experimentation was carried out based on the Ministry of Education, Culture, Sports, Science, and Technology's Fundamental Guidelines for Proper Conduct of Animal Experiments and Related Activities in Academic Research Institutions (Notice No. 71, 2006). This study was approved by the Animal Care and Use Committee of Juntendo University (Approval No. 2024300). No patients or members of the public contributed to the planning, execution, documentation, or sharing of the results of this study.

Conflicts of interest

There are no conflicts to declare.

Data availability

The datasets generated and/or analysed during the current study are available from the corresponding author on reasonable request. AGE used in this study was provided by Wakunaga Pharmaceutical Co., Ltd, and restrictions apply to the availability of this material. Supplementary information (SI) is available. See DOI: https://doi.org/10.1039/d6fo00337k.

Acknowledgements

This work was supported by JSPS KAKENHI Grant Number 25K19469. We thank Wakunaga Pharmaceutical Co., Ltd for the generous gift of AGE. We are also grateful to the staff of the Biomedical Research Core Facilities (Juntendo University Graduate School of Medicine), specifically the Laboratory of Cell Biology and the Laboratory of Morphology and Image Analysis, for providing crucial technical support. We thank Editage (https://www.editage.com) for English language editing. The graphical abstract was created with BioRender.com.

References

1 N. D. Ferguson, E. Fan, L. Camporota, M. Antonelli, A. Anzueto, R. Beale, L. Brochard, R. Brower, A. Esteban, L. Gattinoni, A. Rhodes, A. S. Slutsky, J. L. Vincent, G. D. Rubenfeld, B. T. Thompson and V. M. Ranieri, The Berlin definition of ARDS: an expanded rationale, justification, and supplementary material, *Intensive Care Med.*, 2012, **38**, 1573–1582, DOI: 10.1007/s00134-012-2682-1.

2 M. A. Matthay, Y. Arabi, A. C. Arroliga, G. Bernard, A. D. Bersten, L. J. Brochard, C. S. Calfee, A. Combes, B. M. Daniel, N. D. Ferguson, M. N. Gong, J. E. Gotts, M. S. Herridge, J. G. Laffey, K. D. Liu, F. R. Machado, T. R. Martin, D. F. McAuley, A. Mercat, M. Moss, R. A. Mularski, A. Pesenti, H. Qiu, N. Ramakrishnan, V. M. Ranieri, E. D. Riviello, E. Rubin, A. S. Slutsky, B. T. Thompson, T. Twagirumugabe, L. B. Ware and K. D. Wick, A New Global Definition of Acute Respiratory Distress Syndrome, *Am. J. Respir. Crit. Care Med.*, 2024, **209**, 37–47, DOI: 10.1164/rccm.202303-0558WS.

3 C. Brun-Buisson, M. Fartoukh, E. Lechapt, S. Honoré, J. R. Zahar, C. Cerf and B. Maitre, Contribution of blinded, protected quantitative specimens to the diagnostic and therapeutic management of ventilator-associated pneumonia, *Chest*, 2005, **128**, 533–544, DOI: 10.1378/chest.128.2.533.

4 B. T. Thompson, R. C. Chambers and K. D. Liu, Acute Respiratory Distress Syndrome, *N. Engl. J. Med.*, 2017, **377**, 562–572, DOI: 10.1056/NEJMra1608077.

5 T. B. Deramaudt, M. Ali, S. Vinit and M. Bonay, Sulforaphane reduces intracellular survival of Staphylococcus aureus in macrophages through inhibition of JNK and p38 MAPK-induced inflammation, *Int. J. Mol. Med.*, 2020, **45**, 1927–1941, DOI: 10.3892/ijmm.2020.4563.

6 Y. H. Lin, Y. H. Wang, Y. J. Peng, F. C. Liu, G. J. Lin, S. H. Huang, H. K. Sytwu and C. P. Cheng, Interleukin 26 Skews Macrophage Polarization Towards M1 Phenotype by Activating cJUN and the NF-κB Pathway, *Cells*, 2020, **9**, 938, DOI: 10.3390/cells9040938.

7 C. Yin, J. Cai, Y. Gou, D. Li, H. Tang, L. Wang, H. Liu and B. Luo, Dynamic changes in human THP-1-derived M1-to-M2 macrophage polarization during Thelazia callipaeda MIF induction, *Front. Immunol.*, 2022, **13**, 1078880, DOI: 10.3389/fimmu.2022.1078880.

8 N. Wang, H. Liang and K. Zen, Molecular mechanisms that influence the macrophage m1-m2 polarization balance, *Front. Immunol.*, 2014, **5**, 614, DOI: 10.3389/fimmu.2014.00614.

9 G. Shrivastava, M. León-Juárez, J. García-Cordero, D. E. Meza-Sánchez and L. Cedillo-Barrón, Inflammasomes and its importance in viral infections, *Immunol. Res.*, 2016, **64**, 1101–1117, DOI: 10.1007/s12026-016-8873-z.

10 R. B. Goodman, R. M. Strieter, D. P. Martin, K. P. Steinberg, J. A. Milberg, R. J. Maunder, S. L. Kunkel, A. Walz, L. D. Hudson and T. R. Martin, Inflammatory cytokines in patients with persistence of the acute respiratory distress syndrome, *Am. J. Respir. Crit. Care Med.*, 1996, **154**, 602–611, DOI: 10.1164/ajrccm.154.3.8810593.

11 V. Pooladanda, S. Thatikonda, S. Bale, B. Pattnaik, D. K. Sigalapalli, N. B. Bathini, S. B. Singh and C. Godugu, Nimbolide protects against endotoxin-induced acute respiratory distress syndrome by inhibiting TNF-α mediated NF-κB and HDAC-3 nuclear translocation, *Cell Death Dis.*, 2019, **10**, 81, DOI: 10.1038/s41419-018-1247-9.

12 D. Annane, S. M. Pastores, B. Rochwerg, W. Arlt, R. A. Balk, A. Beishuizen, J. Briegel, J. Carcillo, M. Christ-Crain, M. S. Cooper, P. E. Marik, G. U. Meduri, K. M. Olsen, S. Rodgers, J. A. Russell and G. Van den Berghe, Guidelines for the diagnosis and management of critical illness-related corticosteroid insufficiency (CIRCI) in critically ill patients (Part I): Society of Critical Care Medicine (SCCM) and European Society of Intensive Care Medicine (ESICM) 2017, *Intensive Care Med.*, 2017, **43**, 1751–1763, DOI: 10.1007/s00134-017-4919-5.

13 N. Qadir, S. Sahetya, L. Munshi, C. Summers, D. Abrams, J. Beitler, G. Bellani, R. G. Brower, L. Burry, J. T. Chen, C. Hodgson, C. L. Hough, F. Lamontagne, A. Law, L. Papazian, T. Pham, E. Rubin, M. Siuba, I. Telias, S. Patolia, D. Chaudhuri, A. Walkey, B. Rochwerg and E. Fan, An Update on Management of Adult Patients with Acute Respiratory Distress Syndrome: An Official American Thoracic Society Clinical Practice Guideline, *Am. J. Respir. Crit. Care Med.*, 2024, **209**, 24–36, DOI: 10.1164/rccm.202311-2011ST.

14 S. Tongyoo, C. Permpikul, W. Mongkolpun, V. Vattanavanit, S. Udompanturak, M. Kocak and G. U. Meduri, Hydrocortisone treatment in early sepsis-associated acute respiratory distress syndrome: results of a randomized controlled trial, *Crit. Care*, 2016, **20**, 329, DOI: 10.1186/s13054-016-1511-2.

15 J. Villar, C. Ferrando, D. Martínez, A. Ambrós, T. Muñoz, J. A. Soler, G. Aguilar, F. Alba, E. González-Higueras, L. A. Conesa, C. Martín-Rodríguez, F. J. Díaz-Domínguez, P. Serna-Grande, R. Rivas, J. Ferreres, J. Belda, L. Capilla, A. Tallet, J. M. Añón, R. L. Fernández and J. M. González-Martín, Dexamethasone treatment for the acute respiratory distress syndrome: a multicentre, randomised controlled trial, *Lancet. Respir. Med.*, 2020, **8**, 267–276, DOI: 10.1016/s2213-2600(19)30417-5.

16 D. Chaudhuri, L. Israelian, Z. Putowski, J. Prakash, T. Pitre, A. M. Nei, J. L. Spencer-Segal, H. B. Gershengorn, D. Annane, S. M. Pastores and B. Rochwerg, Adverse Effects Related to Corticosteroid Use in Sepsis, Acute Respiratory Distress Syndrome, and Community-Acquired Pneumonia: A Systematic Review and Meta-Analysis, *Crit. Care Explor.*, 2024, **6**, e1071, DOI: 10.1097/cce.0000000000001071.

17 G. C. Khilnani and V. Hadda, Corticosteroids and ARDS: A review of treatment and prevention evidence, *Lung*, 2011, **28**, 114–119, DOI: 10.4103/0970-2113.80324.

18 E. Kuperminc, N. Heming, M. Carlos and D. Annane, Corticosteroids in ARDS, *J. Clin. Med.*, 2023, **12**, 3340, DOI: 10.3390/jcm12093340.

19 P. J. Andrews, A. Avenell, D. W. Noble, M. K. Campbell, B. L. Croal, W. G. Simpson, L. D. Vale, C. G. Battison, D. J. Jenkinson and J. A. Cook, Randomised trial of glutamine, selenium, or both, to supplement parenteral nutrition for critically ill patients, *Br. Med. J.*, 2011, **342**, d1542, DOI: 10.1136/bmj.d1542.

20 D. Heyland, J. Muscedere, P. E. Wischmeyer, D. Cook, G. Jones, M. Albert, G. Elke, M. M. Berger and A. G. Day, A randomized trial of glutamine and antioxidants in critically ill patients, *N. Engl. J. Med.*, 2013, **368**, 1489–1497, DOI: 10.1056/NEJMoa1212722.

21 M. Nakamoto, K. Kunimura and M. Ohtani, Pharmacokinetics of sulfur?containing compounds in aged garlic extract: S?Allylcysteine, S?1?propenylcysteine, S?methylcysteine, S?allylmercaptocysteine and others (Review), *Exp. Ther. Med.*, 2025, **29**, 102, DOI: 10.3892/etm.2025.12852.

22 T. W. Lee, E. Bae, J. H. Kim, H. N. Jang, H. S. Cho, S. H. Chang and D. J. Park, The aqueous extract of aged black garlic ameliorates colistin-induced acute kidney

injury in rats, *Ren. Fail.*, 2019, **41**, 24–33, DOI: 10.1080/0886022X.2018.1561375.

23 N. Nillert, W. Pannangrong, J. U. Welbat, W. Chaijaroonkhanarak, K. Sripanidkulchai and B. Sripanidkulchai, Neuroprotective Effects of Aged Garlic Extract on Cognitive Dysfunction and Neuroinflammation Induced by β-Amyloid in Rats, *Nutrients*, 2017, **9**, 24, DOI: 10.3390/nu9010024.

24 A. Al-Brakati, Protective effect of aged garlic extracts against hepatotoxicity induced by ethephon in Wistar albino rat, *Environ. Sci. Pollut. Res. Int.*, 2020, **27**, 6139–6147, DOI: 10.1007/s11356-019-07148-w.

25 Y. Kodera, A. Suzuki, O. Imada, S. Kasuga, I. Sumioka, A. Kanezawa, N. Taru, M. Fujikawa, S. Nagae, K. Masamoto, K. Maeshige and K. Ono, Physical, chemical, and biological properties of s-allylcysteine, an amino acid derived from garlic, *J. Agric. Food Chem.*, 2002, **50**, 622–632, DOI: 10.1021/jf0106648.

26 S. Nagae, M. Ushijima, S. Hatono, J. Imai, S. Kasuga, H. Matsuura, Y. Itakura and Y. Higashi, Pharmacokinetics of the garlic compound *S*-allylcysteine, *Planta Med.*, 1994, **60**, 214–217, DOI: 10.1055/s-2006-959461.

27 H. Amano, D. Kazamori, K. Itoh and Y. Kodera, Metabolism, excretion, and pharmacokinetics of *S*-allyl-L-cysteine in rats and dogs, *Drug Metab. Dispos.*, 2015, **43**, 749–755, DOI: 10.1124/dmd.115.063230.

28 W. Chanput, J. J. Mes, H. F. Savelkoul and H. J. Wichers, Characterization of polarized THP-1 macrophages and polarizing ability of LPS and food compounds, *Food Funct.*, 2013, **4**, 266–276, DOI: 10.1039/c2fo30156c.

29 G. Matute-Bello, C. W. Frevert and T. R. Martin, Animal models of acute lung injury, *Am. J. Physiol.: Lung Cell. Mol. Physiol.*, 2008, **295**, L379–L399, DOI: 10.1152/ajplung.00010.2008.

30 P. M. Siegel, A. S. Przewosnik, J. Wrobel, T. Heidt, M. Moser, K. Peter, C. Bode, P. Diehl and I. Bojti, An activation specific anti-Mac-1 designed ankyrin repeat protein improves survival in a mouse model of acute lung injury, *Sci. Rep.*, 2022, **12**, 6296, DOI: 10.1038/s41598-022-10090-6.

31 Y. Nie, K. Yu, B. Li, Y. Hu, H. Zhang, R. Xin, Y. Xiong, P. Zhao and G. Chai, *S*-Allyl-l-cysteine attenuates bleomycin-induced pulmonary fibrosis and inflammation via AKT/NF-κB signaling pathway in mice, *J. Pharmacol. Sci.*, 2019, **139**, 377–384, DOI: 10.1016/j.jphs.2019.03.002.

32 G. Matute-Bello, G. Downey, B. B. Moore, S. D. Groshong, M. A. Matthay, A. S. Slutsky and W. M. Kuebler, An official American Thoracic Society workshop report: features and measurements of experimental acute lung injury in animals, *Am. J. Respir. Cell Mol. Biol.*, 2011, **44**, 725–738, DOI: 10.1165/rcmb.2009-0210ST.

33 D. J. Yeisley, A. S. Arabiyat and M. S. Hahn, Cannabidiol-Driven Alterations to Inflammatory Protein Landscape of Lipopolysaccharide-Activated Macrophages In Vitro May Be Mediated by Autophagy and Oxidative Stress, *Cannabis Cannabinoid Res.*, 2021, **6**, 253–263, DOI: 10.1089/can.2020.0109.

34 S. Takasawa, T. Tateishi, J. Sugihara, S. Shibata, J. Ito, M. Ito, K. Hata, S. Miyake, H. Karasuyama, K. Miyake and Y. Miyazaki, Emerging roles of basophils in the resolution of the acute respiratory distress syndrome, *Eur. Respir. J.*, 2025, **66**, 2401150, DOI: 10.1183/13993003.01150-2024.

35 P. Balbo, M. Silvestri, G. A. Rossi, E. Crimi and S. E. Burastero, Differential role of CD80 and CD86 on alveolar macrophages in the presentation of allergen to T lymphocytes in asthma, *Clin. Exp. Allergy*, 2001, **31**, 625–636, DOI: 10.1046/j.1365-2222.2001.01068.x.

36 A. S. M. Moin, T. Sathyapalan, I. Diboun, S. L. Atkin and A. E. Butler, Identification of macrophage activation-related biomarkers in obese type 2 diabetes that may be indicative of enhanced respiratory risk in COVID-19, *Sci. Rep.*, 2021, **11**, 6428, DOI: 10.1038/s41598-021-85760-y.

37 A. A. Tarique, J. Logan, E. Thomas, P. G. Holt, P. D. Sly and E. Fantino, Phenotypic, functional, and plasticity features of classical and alternatively activated human macrophages, *Am. J. Respir. Cell Mol. Biol.*, 2015, **53**, 676–688, DOI: 10.1165/rcmb.2015-0012OC.

38 Y. Y. Jeong, H. J. Park, Y. W. Cho, E. J. Kim, G. T. Kim, Y. J. Mun, J. D. Lee, J. H. Shin, N. J. Sung, D. Kang and J. Han, Aged red garlic extract reduces cigarette smoke extract-induced cell death in human bronchial smooth muscle cells by increasing intracellular glutathione levels, *Phytother. Res.*, 2012, **26**, 18–25, DOI: 10.1002/ptr.3502.

39 A. Zare, P. Farzaneh, Z. Pourpak, F. Zahedi, M. Moin, S. Shahabi and Z. M. Hassan, Purified aged garlic extract modulates allergic airway inflammation in BALB/c mice, *Iran. J. Allergy, Asthma Immunol.*, 2008, **7**, 133–141.

40 J. Gasparello, C. Papi, G. Marzaro, A. Macone, M. Zurlo, A. Finotti, E. Agostinelli and R. Gambari, Aged Garlic Extract (AGE) and Its Constituent *S*-Allyl-Cysteine (SAC) Inhibit the Expression of Pro-Inflammatory Genes Induced in Bronchial Epithelial IB3-1 Cells by Exposure to the SARS-CoV-2 Spike Protein and the BNT162b2 Vaccine, *Molecules*, 2024, **29**, 5938, DOI: 10.3390/molecules29245938.

41 E. Agostinelli, G. Marzaro, R. Gambari and A. Finotti, Potential applications of components of aged garlic extract in mitigating pro-inflammatory gene expression linked to human diseases (Review), *Exp. Ther. Med.*, 2025, **30**, 134, DOI: 10.3892/etm.2025.12884.

42 S. I. Ali, A. M. E. Elkhalifa, S. U. Nabi, F. S. Hayyat, M. Nazar, S. Taifa, R. Rakhshan, I. H. Shah, M. Shaheen, I. A. Wani, U. Muzaffer, O. S. Shah, D. M. Makhdoomi, E. M. Ahmed, K. A. A. Khalil, E. A. Bazie, K. I. Zawbaee, M. M. Al Hasan Ali, R. J. Alanazi, I. A. Al Bataj, S. M. Al Gahtani, A. J. Salwi and L. S. Alrodan, Aged garlic extract preserves beta-cell functioning via modulation of nuclear factor kappa-B (NF-κB)/Toll-like receptor (TLR)-4 and sarco endoplasmic reticulum calcium ATPase (SERCA)/Ca(2+) in diabetes mellitus, *Diabetol. Metab. Syndr.*, 2024, **16**, 110, DOI: 10.1186/s13098-024-01350-8.

43 J. H. Ryu, H. J. Park, Y. Y. Jeong, S. Han, J. H. Shin, S. J. Lee, M. J. Kang, N. J. Sung and D. Kang, Aged red

garlic extract suppresses nitric oxide production in lipopolysaccharide-treated RAW 264.7 macrophages through inhibition of NF-κB, *J. Med. Food*, 2015, **18**, 439–445, DOI: 10.1089/jmf.2014.3214.

44 C. Basu, A. Chatterjee, S. Bhattacharya, N. Dutta and R. Sur, *S*-Allyl cysteine inhibits TNF-α-induced inflammation in HaCaT keratinocytes by inhibition of NF- κB-dependent gene expression via sustained ERK activation, *Exp. Dermatol.*, 2019, **28**, 1328–1335, DOI: 10.1111/exd.14041.

45 T. Rőszer, Understanding the Mysterious M2 Macrophage through Activation Markers and Effector Mechanisms, *Mediators Inflammation*, 2015, **2015**, 816460, DOI: 10.1155/2015/816460.

46 S. Miki, J. I. Suzuki, M. Takashima, M. Ishida, H. Kokubo and M. Yoshizumi, *S*-1-Propenylcysteine promotes IL-10-induced M2c macrophage polarization through prolonged activation of IL-10R/STAT3 signaling, *Sci. Rep.*, 2021, **11**, 22469, DOI: 10.1038/s41598-021-01866-3.

47 L. Meng, X. Liao, Y. Wang, L. Chen, W. Gao, M. Wang, H. Dai, N. Yan, Y. Gao, X. Wu, K. Wang and Q. Liu, Pharmacologic therapies of ARDS: From natural herb to nanomedicine, *Front. Pharmacol.*, 2022, **13**, 930593, DOI: 10.3389/fphar.2022.930593.

48 K. C. Meyer, Immunosuppressive agents and interstitial lung disease: what are the risks?, *Expert Rev. Respir. Med.*, 2014, **8**, 263–266, DOI: 10.1586/17476348.2014.880054.

49 K. Nagai, Immunosuppressive Agent Options for Primary Nephrotic Syndrome: A Review of Network Meta-Analyses and Cost-Effectiveness Analysis, *Medicina (Kaunas)*, 2023, **59**, 601, DOI: 10.3390/medicina59030601.

50 G. Bellani, J. G. Laffey, T. Pham, E. Fan, L. Brochard, A. Esteban, L. Gattinoni, F. van Haren, A. Larsson, D. F. McAuley, M. Ranieri, G. Rubenfeld, B. T. Thompson, H. Wrigge, A. S. Slutsky and A. Pesenti, Epidemiology, Patterns of Care, and Mortality for Patients With Acute Respiratory Distress Syndrome in Intensive Care Units in 50 Countries, *J. Am. Med. Assoc.*, 2016, **315**, 788–800, DOI: 10.1001/jama.2016.0291.

51 L. Papazian, V. Pauly, I. Hamouda, F. Daviet, V. Orleans, J. M. Forel, A. Roch, S. Hraiech and L. Boyer, National incidence rate and related mortality for acute respiratory distress syndrome in France, *Anaesth. Crit. Care Pain Med.*, 2021, **40**, 100795, DOI: 10.1016/j.accpm.2020.100795.

52 L. Pisani, A. G. Algera, A. S. Neto, L. Azevedo, T. Pham, F. Paulus, M. G. de Abreu, P. Pelosi, A. M. Dondorp, G. Bellani, J. G. Laffey and M. J. Schultz, Geoeconomic variations in epidemiology, ventilation management, and outcomes in invasively ventilated intensive care unit patients without acute respiratory distress syndrome: a pooled analysis of four observational studies, *Lancet. Glob. Health*, 2022, **10**, e227–e235, DOI: 10.1016/s2214-109x(21)00485-x.